

pubs.acs.org/NanoLett Letter

Excitonic Effect Drives Ultrafast Dynamics in van der Waals Heterostructures

Junyi Liu, Xu Zhang, and Gang Lu*



Cite This: Nano Lett. 2020, 20, 4631-4637



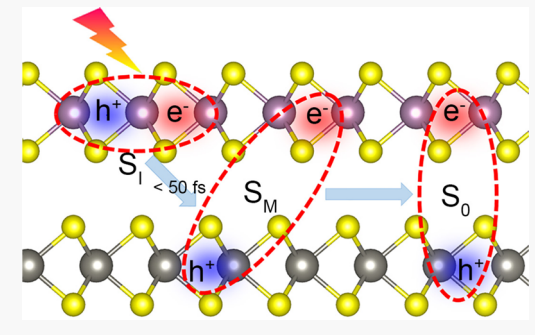
ACCESS I

III Metrics & More

Article Recommendations

Supporting Information

ABSTRACT: Recent experiments revealed stacking-configuration-independent and ultrafast charge transfer in transition metal dichalcogenides van der Waals (vdW) heterostructures, which is surprising given strong exciton binding energies and large momentum mismatch across the heterojunctions. Previous theories failed to provide a comprehensive physical picture for the charge transfer mechanisms. To address this challenge, we developed a first-principles framework which can capture exciton-phonon interaction in extended systems. We find that excitonic effect does not impede, but actually drives ultrafast charge transfer in vdW heterostructures. The many-body electron-hole interaction affords cooperation among the electrons, which relaxes the constraint on momentum conservation and reduces energy gaps for charge transfer. We uncover a two-step process in exciton dynamics: ultrafast hole transfer followed



by much longer relaxation of intermediate "hot" excitons. This work establishes that many-body excitonic effect is crucial to the ultrafast dynamics and provides a basis to understand relevant phenomena in vdW heterostructures.

KEYWORDS: Exciton, vdW heterostructures, ultrafast dynamics, TD-DFT

Van der Waals (vdW) heterostructures are synthetic quantum materials composed of two-dimensional (2D) layers assembled vertically through vdW interactions. Many fascinating electronic, optical, and magnetic properties have been reported or envisioned in vdW heterostructures, including fractal quantum Hall effect, 1,2 topological insulators, unconventional superconductivity, superfluidity, etc. As the most widely studied 2D semiconductors, transition metal dichalcogenides (TMDs) and their heterostructures feature prominent excitonic effect with large exciton binding energy in the range of 0.3 to 1.1 eV, $^{6-10}$ owing to quantum confinement and reduced dielectric screening. $^{11-13}$

Most TMD heterostructures adopt type II band alignment, which hosts long-lived interlayer excitons with electron and hole separated at different layers. The remarkably strong lightmatter interactions in TMDs combined with the type II alignment give rise to a myriad of novel physical phenomena 14-18 and promising optoelectronic applications, 19,20 such as photovoltaics and nanophotonics. Recent pump-probe spectroscopy experiments have revealed ultrafast charge transfer in TMD heterostructures.²¹ Hong et al. was the first to report that, in MoS₂/WS₂ heterostructure, holes can transfer from MoS₂ to WS₂ within 50 fs after selective excitation of MoS_2 .²² Similar ultrafast charge transfer was also observed in other TMD heterostructures.^{23–26} The most surprising result was that the ultrafast charge transfer exhibited no dependence on interlayer stacking configurations and insensitivity to temperature. 21,22,27 These experimental observations have raised a number of important questions that are yet to be

answered. Chief among them is the physical origin of ultrafast charge transfer in spite of large exciton binding energies and apparent lack of momentum conservation when charge transfers across an artificially stacked heterojunction with a large momentum change.²⁸ Both are expected to impede charge transfer.

To understand the unexpected ultrafast charge transfer in the TMD heterostructures, several first-principles nonadiabatic molecular dynamics (NAMD) simulations have been performed.^{29–34} Although these studies shed light into the charge transfer processes, none of them incorporated many-body excitonic effect in the simulations. As a result, a complete picture of charge transfer mechanisms remains elusive. Indeed, it has been recognized that "the mechanisms developed to date do not fully account for the Coulombic interactions between electrons and holes, despite the existence of strongly bound excitons both in the TMD monolayers and the heterostructures". 21 Furthermore, theoretical charge transfer time scales were often much longer than the experimental values or exhibited strong dependence on stacking configurations and/or temperature.

Received: April 9, 2020 Revised: May 19, 2020 Published: May 20, 2020





The conventional first-principles approach that incorporates excitonic effect in semiconductors is the GW-Bethe-Salpeter equation (GW-BSE) method based on many-body perturbation theory. 35-37 However, the GW-BSE approach is prohibitively expensive when combined with NAMD simulations. In this paper, we develop and employ a first-principles framework to predict exciton dynamics in solids, which is computationally much more expeditious than GW-BSE. First, ab initio Born-Oppenheimer Molecular Dynamics (BOMD) is performed for the MoS₂/WS₂ heterostructure. At each BOMD time step, a linear-response time-dependent density functional theory (LR-TDDFT)^{38,39} calculation is carried out using an optimally tuned, screened, and range-separated hybrid exchange-correlation functional (OT-SRSH)⁴⁰⁻⁴³ implemented in conjunction with planewaves and pseudopotentials. 44-48 The excitation energies and oscillator strengths are determined to construct time-dependent many-body wave functions based on single Slater determinants, 49 following the assignment ansatz of Casida. 50 The time-dependent excitonic wave functions are then expanded in terms of these many-body wave functions, with the expansion coefficients computed from the fewest-switches-surface-hopping (FSSH) NAMD simulations. 51-53 The exciton is assumed to occupy an initial manybody state, and each coefficient represents the probability amplitude for an excitonic transition from the initial state to a given many-body state. The phonon-assisted excitonic transitions are captured by the nonadiabatic coupling matrix which depends on the time-dependent many-body wave functions and excitation energies of the system. 49,54,55 The details of the method can be found in the Supporting Information (section S2). This proposed computational framework paves the way for probing exciton-phonon interaction in solids and to the best of our knowledge represents the first study of exciton dynamics in 2D vdW heterostructures from first principles. We reveal that the excitonic effect does not impede, but actually drives ultrafast charge transfer. The many-body electron-hole interaction affords cooperation between the electrons, which relaxes the constraint on momentum conservation of independent particles and more importantly reduces the energy gaps for charge transfer. We uncover a two-step dynamic process: an ultrafast hole transfer followed by a much longer relaxation of intermediate "hot" excitons, in good agreement with experiments. In the presence of excitonic effect, ultrafast hole transfer is found to be independent of stacking configurations and temperature. Interestingly, the opposite is found when the excitonic effect is neglected. This work thus establishes that the many-body excitonic effect, previously ignored, is in fact crucial to ultrafast dynamics in vdW heterostructures.

As shown in Figure S2a, an orthogonal (3×3) supercell with 108 atoms is used to model the MoS_2/WS_2 heterostructure. A vacuum slab of 15 Å along the z-direction is adopted to minimize spurious interactions from the periodic images. After structure relaxations, ab initio Born–Oppenheimer molecular dynamic (BOMD) simulation is followed to bring the temperature of the system to a specific temperature with a velocity rescaling method. Then, the temperature is kept for 5 ps to reach the thermal equilibrium. Finally, a microcanonical BOMD production run is performed for 5000 fs with a time step of 1 fs. At each MD step, the excitation energies and the many-body wave functions are determined based on TDDFT-OT-SRSH calculations. Using the microcanonical BOMD trajectory, the population of each

exciton as a function of time is calculated by averaging 4×10^5 NAMD trajectories, each of which is 1000 fs long. The structural relaxation and ab initio BOMD simulations are performed with the Vienna ab initio Simulation Package (VASP), 56 using projector-augmented-wave potentials 57 with a cutoff energy of 400 eV and generalized gradient approximations in Perdew-Burke-Ernzerhof (PBE)⁵⁸ form for the exchange correlation functional. The semiempirical DFT-D2 method⁵⁹ is used to account for the van der Waals (vdW) interaction between the MoS2 and WS2 layers. We have also included spin-orbit coupling (SOC) on the calculations of the band structures of MoS₂/WS₂ heterostructures using HSE06 functionals (section S6). We find that SOC has little effect on the orbital hybridization. More importantly, we reveal that SOC could further reduce the energy gaps for ultrafast charge transfer, thus supporting the main conclusion of the paper.

We use the MoS_2/WS_2 bilayer as an example of 2D vdW heterostructures, for which experimental and theoretical data are available for comparison. As the first validation of the theoretical framework, we compute the fundamental gap $(E_{\rm g})$ and optical gap $(E_{\rm opt})$ of each monolayer using time-independent and time-dependent DFT with the OT-SRSH functional, respectively. All these gap values agree very well with the experimental or GW results, as shown in Table S1, indicating the reliability of the (TD)DFT-OT-SRSH method for the systems in hand. The exciton binding energy defined as $E_{\rm b}=E_{\rm g}-E_{\rm opt}$ is estimated as 0.71 and 0.65 eV for monolayer MoS₂ and WS₂, respectively, confirming the strong excitonic effect.

We next focus on the MoS_2/WS_2 heterostructure in C7 stacking, which is energetically the most stable structure. ⁶⁰ Its band structure calculated with the PBE functional ⁵⁸ is presented in Figure 1a, where the conduction band minimum

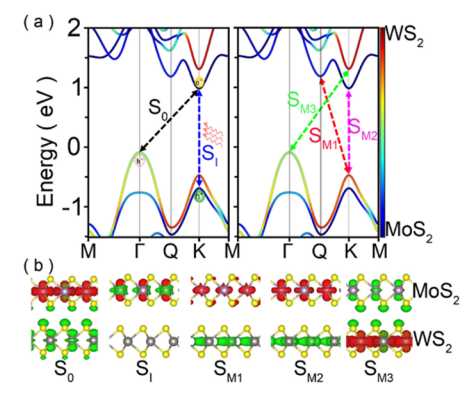


Figure 1. (a) Band structure of MoS_2/WS_2 heterostructure in C7 stacking (left and right). The projection of each band onto WS_2 (deep red) and MoS_2 (deep blue) is color-coded according to the side bar. (b) The charge density distribution of each exciton with red and green color representing quasi-electron and hole, respectively. The iso-surface value is set at $3.5 \times 10^{-4} \text{ Å}^{-3}$.

(CBM) and valence band maximum (VBM) at K valley resides on MoS_2 and WS_2 , respectively, confirming the type II band alignment. Moreover, the interlayer hybridization varies considerabley across the Brillouin zone. In particular, the interlayer coupling at the K valley is weaker than that at the Γ valley, revealed by the color scheme. If the single-particle picture were valid, one would conclude that charge transfer at the K valley should be slower than that at the Γ valley. Similarly, across a twisted or displaced heterostructure, there is

a momentum shift to the single-particle state and variation of interlayer coupling, thus charge transfer rate. Hence, one would expect a strong dependence of charge transfer on stacking configurations based on the single-particle picture, which unfortunately contradicts with the experimental observations. Both erroneous expectations are actually what the previous first-principles studies have found by ignoring the excitonic effect.

We first perform LR-TDDFT calculations with OT-SRSH to examine the static properties of the excitons. The MoS₂/WS₂ heterostructure is modeled by a 3 × 3 supercell with 108 atoms. Although only the Γ point is sampled in the Brillouin zone, several irreducible k-points in the primitive unit cell can be included by unfolding the energy bands of the 3×3 supercell,³⁰ and the details of the energy band assignment can be found in the Supporting Information (section S4). We focus on five low-energy excitons whose charge densities are shown in Figure 1: (i) S_I is an intralayer exciton whose electron and hole occupy the K valley of MoS₂. S₁ is the initial excitation that is generated by laser pumps in the pump-probe experiments. 22,61 The energy of S_I is computed as 1.83 eV, in excellent agreement with the energy (1.86 eV) of the A exciton in MoS₂.61 (ii) S₀ is an interlayer exciton whose electron is primarily composed of CBM at the K valley of MoS₂ (MoS₂@K) and hole of VBM at the Γ valley of WS₂, respectively. So is the lowest-energy exciton in the heterostructure (1.48 eV). (iii-v) S_{M1}, S_{M2}, and S_{M3} are three intermediate interlayer excitons whose energy is 1.85, 1.74, and 1.80 eV, respectively. As elucidated below, exciton-phonon interaction is reponsible for the ultrafast charge transfer in MoS₂/WS₂ heterostructure driven by an energetic relaxation from the initial state (S_I) to the final state (S₀) via the intermediate states (S_{M1} , S_{M2} , and S_{M3}).

We subsequently performed NAMD simulations at 100 and 300 K to determine the population of each exciton as a function of time, shown in Figure 2a and b. At both temperatures, the population of the initial intralayer exciton (S_I) decays drastically and simultaneously the populations of the intermediate interlayer excitons (S_{M1}, S_{M2}, S_{M3}) rise rapidly. The transition from the intralayer exciton to the interlayer excitons is accompanied by the hole transfer from MoS₂ to WS₂. The decaying and rising (S_{M1}) curves cross at 42 and 48 fs for 100 and 300 K, respectively, demonstrating ultrafast hole transfer, as observed experimentally.²² At both temperatures, the hole transfer takes place within 50 fs, displaying weak temperature dependence of charge transfer, consistent with the experiments.^{22,27} Over a much longer time scale, the lowestenergy interlayer exciton S₀ overtakes the intermediate excitons in population. The two-step process, i.e., the ultrafast hole transfer followed by the relaxation of the intermediate "hot" excitons to the lowest-energy interlayer exciton has also been observed experimentally.⁶¹ In particular, the relaxation time scale measured experimentally was ~800 fs at room temperature, which agrees well with our NAMD results that the lowest-energy interlayer exciton S₀ overtakes the other excitons after 600 fs at 300 K. The formation of the S_{M3} exciton is interesting for two reasons: (1) it represents ultrafast but transient energy transfer, as electron and hole transfer simultaneously across the layers. The competition between charge and energy transfer in vdW heterostructures is of significant current interest, 21 and the proposed theoretical framework lays the foundation for future work in this area. (2) The transition of $S_I \rightarrow S_{M3} \rightarrow S_0$ is accompanied by electron

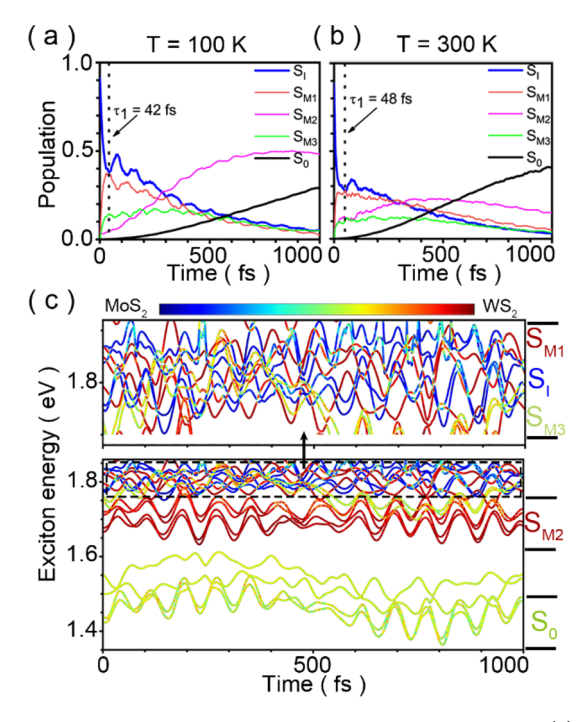


Figure 2. Population of each exciton as a function of time at (a) 100 K and (b) 300 K. (c) The energy of the excitons as a function of time at 100 K. The projection of the hole density onto WS_2 (deep red) and MoS_2 (deep blue) for each exciton is color-coded according to the top bar. The upper panel is a blown-up view of the dashed box in the lower panel.

transfer from MoS_2 to WS_2 and back to MoS_2 . This recoil of the excited electron across the layers has recently been suggested as a new pathway for hot electron relaxation in MoS_2/WSe_2 . The competition/cooperation between electron—phonon and electron—hole interaction is responsible for the intriguing dynamics of the excited electrons.

To elucidate the origin of ultrafast hole transfer, we examine exciton energy as a function of time in Figure 2c. The upper panel is a blown-up view of the dashed box in the lower panel. Thermal fluctuations at 100 K break the symmetries and energy degeneracy at 0 K. In the energy range of 1.75-1.85 eV, the initial exciton S_I splits into four different excitonic states, represented by the blue curves. Similarly, the lowest energy exciton S₀ breaks into two different states around 1.45 eV, indicated by the green curves. Inside the dashed box, the red curves represent the intermediate exciton S_{M1} and the two light green curves represent S_{M3}. Below the dashed box, four additional deep red curves correspond to $S_{\rm M2}$. Clearly, there are strong energy overlaps among S_{ν} , S_{M1} , and S_{M3} at 100 K, which enable adiabatic and ultrafast charge transfer as shown in Figure 2a. On the other hand, there is no energy crossing between the intermediate excitons and S₀, leading to a nonadiabatic and much slower ("hot" exciton) relaxation process.

The vibrational modes that contribute to the adiabatic excitonic transitions can be obtained by Fourier transform (FT) of the time-dependent exciton energy evolution. As shown in Figure 3, the initial exciton S_1 and the intermediate state $S_{\rm M1}/S_{\rm M2}/S_{\rm M3}$ are strongly coupled to phonons around $\sim 400~{\rm cm}^{-1}$, which correspond to primarily the out-of-plane $A_{\rm 1g}$ optical modes of MoS_2 (404 cm⁻¹) and WS_2 (420 cm⁻¹). Thus, the vibrations of S atoms perpendicular to the interface give rise to the ultrafast exciton transition. In other words, the

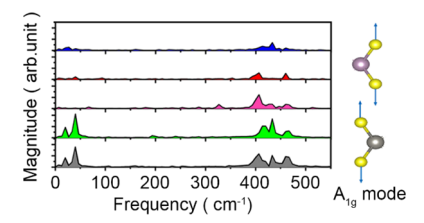


Figure 3. Fourier transform (FT) of the time-dependent energy evolution for each exciton. The schematic of A_{1g} vibrational mode for MoS_2 and WS_2 monolayer is shown in the right panel.

dynamics of the intermediate excitons, with electrons and holes at different valleys, results from intervalley scattering assisted by the optical phonons with high frequencies. The exciton—phonon interaction is also manifest by the fact that the population of momentum-conserving exciton ($S_{\rm M2}$) dominates that of momentum nonconserving excitons ($S_{\rm M1}$ and $S_{\rm M3}$), especially at 100 K, as shown in Figure 2a.

To accentuate the excitonic effect on charge transfer, we also performed similar calculations as in previous work without considering the excitonic effect. To this end, ground state DFT, as opposed to LR-TDDFT, calculations with the same OT-SRSH functional are carried out at each BOMD time step. The single-particle KS orbitals and energies are obtained, and time-dependent single-particle wave functions of the "excited" electron (or hole) are expanded in terms of the KS orbitals. These time-dependent expansion coefficients are determined from the FSSH-NAMD simulations, and each coefficient represents the probability amplitude of the electron (or hole) that occupies one of the KS orbitals. The photoexcited hole starts out at the K valley of MoS_2 , and it then transfers to WS_2 (K valley) and finally relaxes to the Γ valley of WS_2 . Using the standard exponential fitting shown in Figure 4a, we estimate

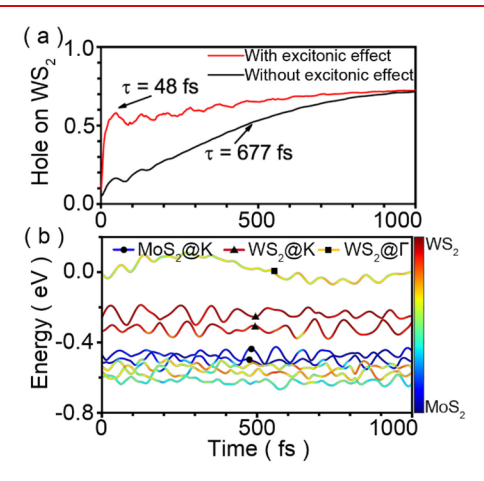


Figure 4. (a) Time evolution of the hole population on WS_2 with and without considering excitonic effect. (b) Time evolution of the KS energy levels near VBM. The hole localization of each KS state on WS_2 or MS_2 is color-coded according to the side bar.

the hole transfer time as 677 fs at 300 K. This charge transfer time (and mechanism) is similar to that (350 fs) found in the previous work³⁰ based on the single-particle picture, but much longer than the experimental value (<50 fs) as well as our result (48 fs) with the excitonic effect included. The time evolution of the KS energies near VBM is shown in Figure 4b, and owing to large separations between the single-particle energy levels, there is no energy overlap between the hole

states at the MoS₂ K valley (MoS₂@K) and WS₂ K valley (WS₂@K), nor is there one between WS₂@K and WS₂@Γ during the BOMD simulations. The energy separation between MoS₂@K and WS₂@K, ΔE_K , is 0.18 eV based on DFT-OT-SRSH calculations at 0 K, which is much larger than the energy separation between the many-body excitonic states S₁ and S_{M1} ($\Delta S = 0.02$ eV) from LR-TDDFT-OT-SRSH calculations. Therefore, in the single-particle picture, the interlayer hole transfer is dominated by nonadiabatic transitions. In contrast, the many-body excitonic effect enables the ultrafast hole transfer mediated by adiabatic transitions. The comparisons here explain why the previous efforts failed to reproduce the experimental results even when hybrid functionals were included in the ground state DFT calculations.

Finally, we address charge transfer dependence on stacking configurations. We have examined exciton dynamics in three different stacking configurations (C7-t, T, and T-t), which have slightly higher energies than C7 stacking. Compared with C7 stacking, T stacking involves an interlayer rotation. C7-t (T-t) stacking can be obtained by interlayer translation from C7 (T) stacking. The atomic and band structures of the stackings are shown in the Supporting Information. The energies of the excitons (S_0 , S_1 , S_{M1} , S_{M2} , and S_{M3}) are summarized in Table 1,

Table 1. Energy (eV) of S_1 , S_{M1} , S_{M2} , S_{M2} , and S_0 in Different Stacking Configurations^a

	with excitonic effect							single particle
stacking	S ₀	S_{I}	S_{M1}	S_{M2}	S_{M3}	СТ	ΔS	$\Delta E_{ m K}$
C7	1.48	1.83	1.85	1.74	1.80	42	0.02	0.18
C7-t	1.45	1.80	1.86	1.73	1.77	43	0.03	0.15
T	1.41	1.81	1.82	1.69	1.79	31	0.01	0.30
T-t	1.48	1.80	1.89	1.80	1.73	42	0.0	0.10

 $^a\Delta S$ is the minimal energy difference between $S_{\rm I}$ and $S_{\rm M1}/S_{\rm M2}/S_{\rm M3}.$ $\Delta E_{\rm K}$ represents the energy difference between the hole states at MoS_2@K and WS_2@K at 0 K. CT is the calculated charge transfer time (fs) at 100 K.

showing weak dependence on the stacking configurations. An exciton state is a superposition of many single-particle excitations between different k-valleys. Although each singleparticle excitation may depend sensitively on the stacking configurations, their superpositions are more robust against the variation of interlayer stackings. The energy differences between the three intermediate excitons $(S_{M1}, S_{M2}, \text{ and } S_{M3})$ are very small in each stacking configuration. More importantly, the minimal energy difference (ΔS) between the initial intralayer exciton S_I and the three intermediate interlayer excitons is less than 0.03 eV for all stacking configurations, suggesting that thermal fluctuation at 300 K could easily surmount ΔS for charge transfer. In sharp contrast, the energy difference between the hole states at MoS₂@K and WS₂@K $(\Delta E_{\rm K})$ is 1 order of magnitude larger than ΔS for all stacking configurations.

The NAMD results for the three different stacking configurations at 100 K are shown in Figure 5a–c. Similar to C7 stacking, the initial intralayer exciton S_1 transfers into the intermediate excitons within 50 fs and then relaxes to the lowest interlayer exciton S_0 with a much slower rate. Again, strong energy overlaps between the excitonic states are found in all three stacking configurations, as shown in Figure 5d–f. Thus, we confirm the experimental observations of robust and

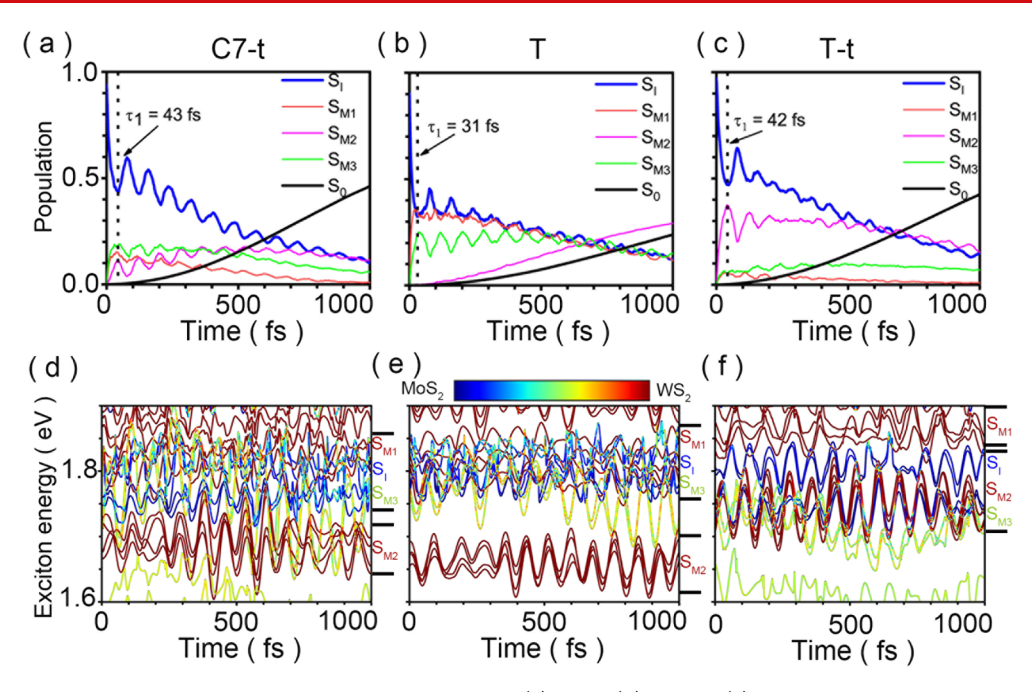


Figure 5. Population of each exciton as a function of time at 100 K in (a) C7-t, (b) T, and (c) T-t stacking configuration. The corresponding energy of the excitons as a function of time at 100 K is in (d) C7-t, (e) T, and (f) T-t stacking configuration. The projection of the hole density onto WS_2 (deep red) and MOS_2 (deep blue) for each exciton is color-coded according to the top bar.

ultrafast charge transfer, independent of stacking configura-

To conclude, we develop a first-principles framework which captures exciton-phonon interaction responsible for exciton dynamics in the vdW heterostructures. By taking the MoS₂/ WS₂ heterostructure as the prototype system, we reveal that the many-body excitonic effect drives ultrafast and stackingconfiguration-independent charge transfer. On the one hand, many-body interaction enables cooperation among the electrons, which reduces the energy separations between the excitonic states. In contrast, lacking this cooperation, the energy separations between the corresponding single-particle states are significantly larger, yielding much slower charge transfer rates and strong dependence on stacking configurations and temperature. On the other hand, the cooperation between electron and hole relaxes the requirement of momentum conservation. In the single-particle picture, the momentum conservation must be satisfied on an individual electron and hole. In the many-body picture, it is on excitons—the electron and hole could change its momentum independently if their sum is conserved. Therefore, momentum conservation can be satisfied more easily. Given the strong exciton binding energy in 2D materials, this electron-hole cooperated dynamic would be general in vdW heterostructures. This work not only provides a coherent and comprehensive physical picture for ultrafast dynamics in vdW heterostructures but also lays the foundation to understand other relevant phenomena in this fascinating family of materials.

ASSOCIATED CONTENT

Supporting Information

The Supporting Information is available free of charge at https://pubs.acs.org/doi/10.1021/acs.nanolett.0c01519.

Additional data and figures including MoS₂/WS₂ heterostructure in different stacking configurations;

computational details of NAMD methods; parameters test for OT-SRSH functional; band unfolding; time evolution of the exciton states at 300 K; spin—orbit coupling (SOC) effect (PDF)

AUTHOR INFORMATION

Corresponding Author

Gang Lu − Department of Physics and Astronomy, California State University Northridge, California 91330-8268, United States; orcid.org/0000-0002-9168-8968; Email: ganglu@csun.edu

Authors

Junyi Liu — Department of Physics and Astronomy, California State University Northridge, California 91330-8268, United States; ⊙ orcid.org/0000-0002-2018-1668

Xu Zhang — Department of Physics and Astronomy, California State University Northridge, California 91330-8268, United States; orcid.org/0000-0002-6491-3234

Complete contact information is available at: https://pubs.acs.org/10.1021/acs.nanolett.0c01519

Notes

The authors declare no competing financial interest.

■ ACKNOWLEDGMENTS

The work was supported by the National Science Foundation (DMR1828019) and the Army Research Office (W911NF1810473). The discussion with Zi Li is greatly appreciated.

REFERENCES

(1) Dean, C. R.; Wang, L.; Maher, P.; Forsythe, C.; Ghahari, F.; Gao, Y.; Katoch, J.; Ishigami, M.; Moon, P.; Koshino, M. Hofstadter's butterfly and the fractal quantum Hall effect in moiré superlattices. *Nature* **2013**, 497 (7451), 598–602.

- (2) Wang, L.; Gao, Y.; Wen, B.; Han, Z.; Taniguchi, T.; Watanabe, K.; Koshino, M.; Hone, J.; Dean, C. R. Evidence for a fractional fractal quantum Hall effect in graphene superlattices. *Science* **2015**, *350* (6265), 1231–1234.
- (3) Spanton, E. M.; Zibrov, A. A.; Zhou, H.; Taniguchi, T.; Watanabe, K.; Zaletel, M. P.; Young, A. F. Observation of fractional Chern insulators in a van der Waals heterostructure. *Science* **2018**, *360* (6384), 62–66.
- (4) Cao, Y.; Fatemi, V.; Fang, S.; Watanabe, K.; Taniguchi, T.; Kaxiras, E.; Jarillo-Herrero, P. Unconventional superconductivity in magic-angle graphene superlattices. *Nature* **2018**, *556* (7699), 43–50.
- (5) Fogler, M.; Butov, L.; Novoselov, K. High-temperature superfluidity with indirect excitons in van der Waals heterostructures. *Nat. Commun.* **2014**, 5 (1), 1–5.
- (6) Hill, H. M.; Rigosi, A. F.; Roquelet, C.; Chernikov, A.; Berkelbach, T. C.; Reichman, D. R.; Hybertsen, M. S.; Brus, L. E.; Heinz, T. F. Observation of excitonic Rydberg states in monolayer MoS₂ and WS₂ by photoluminescence excitation spectroscopy. *Nano Lett.* **2015**, *15* (5), 2992–2997.
- (7) Chernikov, A.; Berkelbach, T. C.; Hill, H. M.; Rigosi, A.; Li, Y.; Aslan, O. B.; Reichman, D. R.; Hybertsen, M. S.; Heinz, T. F. Exciton binding energy and nonhydrogenic Rydberg series in monolayer WS₂. *Phys. Rev. Lett.* **2014**, *113* (7), 076802.
- (8) Shi, H.; Pan, H.; Zhang, Y.-W.; Yakobson, B. I. Quasiparticle band structures and optical properties of strained monolayer MoS 2 and WS 2. *Phys. Rev. B: Condens. Matter Mater. Phys.* **2013**, 87 (15), 155304.
- (9) Ramasubramaniam, A. Large excitonic effects in monolayers of molybdenum and tungsten dichalcogenides. *Phys. Rev. B: Condens. Matter Mater. Phys.* **2012**, *86* (11), 115409.
- (10) Qiu, D. Y.; da Jornada, F. H.; Louie, S. G. Optical spectrum of MoS 2: many-body effects and diversity of exciton states. *Phys. Rev. Lett.* **2013**, *111* (21), 216805.
- (11) Cudazzo, P.; Attaccalite, C.; Tokatly, I. V.; Rubio, A. Strong charge-transfer excitonic effects and the Bose–Einstein exciton condensate in graphane. *Phys. Rev. Lett.* **2010**, *104* (22), 226804.
- (12) Olsen, T.; Latini, S.; Rasmussen, F.; Thygesen, K. S. Simple screened hydrogen model of excitons in two-dimensional materials. *Phys. Rev. Lett.* **2016**, *116* (5), 056401.
- (13) Wirtz, L.; Marini, A.; Rubio, A. Excitons in boron nitride nanotubes: dimensionality effects. *Phys. Rev. Lett.* **2006**, *96* (12), 126104.
- (14) Tran, K.; Moody, G.; Wu, F.; Lu, X.; Choi, J.; Kim, K.; Rai, A.; Sanchez, D. A.; Quan, J.; Singh, A. Evidence for moiré excitons in van der Waals heterostructures. *Nature* **2019**, *567* (7746), 71–75.
- (15) Yu, H.; Liu, G.-B.; Tang, J.; Xu, X.; Yao, W. Moiré excitons: From programmable quantum emitter arrays to spin-orbit-coupled artificial lattices. *Sci. Adv.* **2017**, *3* (11), No. e1701696.
- (16) Kim, J.; Jin, C.; Chen, B.; Cai, H.; Zhao, T.; Lee, P.; Kahn, S.; Watanabe, K.; Taniguchi, T.; Tongay, S. Observation of ultralong valley lifetime in WSe₂/MoS₂ heterostructures. *Sci. Adv.* **2017**, *3* (7), No. e1700518.
- (17) Rivera, P.; Seyler, K. L.; Yu, H.; Schaibley, J. R.; Yan, J.; Mandrus, D. G.; Yao, W.; Xu, X. Valley-polarized exciton dynamics in a 2D semiconductor heterostructure. *Science* **2016**, *351* (6274), 688–691.
- (18) Rivera, P.; Schaibley, J. R.; Jones, A. M.; Ross, J. S.; Wu, S.; Aivazian, G.; Klement, P.; Seyler, K.; Clark, G.; Ghimire, N. J. Observation of long-lived interlayer excitons in monolayer MoSe₂-WSe₂ heterostructures. *Nat. Commun.* **2015**, *6* (1), 1–6.
- (19) Withers, F.; Del Pozo-Zamudio, O.; Mishchenko, A.; Rooney, A.; Gholinia, A.; Watanabe, K.; Taniguchi, T.; Haigh, S.; Geim, A.; Tartakovskii, A. Light-emitting diodes by band-structure engineering in van der Waals heterostructures. *Nat. Mater.* **2015**, *14* (3), 301–306.
- (20) Bernardi, M.; Palummo, M.; Grossman, J. C. Extraordinary sunlight absorption and one nanometer thick photovoltaics using two-dimensional monolayer materials. *Nano Lett.* **2013**, *13* (8), 3664–3670.

- (21) Jin, C.; Ma, E. Y.; Karni, O.; Regan, E. C.; Wang, F.; Heinz, T. F. Ultrafast dynamics in van der Waals heterostructures. *Nat. Nanotechnol.* **2018**, *13* (11), 994–1003.
- (22) Hong, X.; Kim, J.; Shi, S.-F.; Zhang, Y.; Jin, C.; Sun, Y.; Tongay, S.; Wu, J.; Zhang, Y.; Wang, F. Ultrafast charge transfer in atomically thin MoS₂/WS₂ heterostructures. *Nat. Nanotechnol.* **2014**, *9* (9), 682–686.
- (23) Li, Y.; Cui, Q.; Ceballos, F.; Lane, S. D.; Qi, Z.; Zhao, H. Ultrafast interlayer electron transfer in incommensurate transition metal dichalcogenide homobilayers. *Nano Lett.* **2017**, *17* (11), 6661–6666
- (24) Ceballos, F.; Bellus, M. Z.; Chiu, H.-Y.; Zhao, H. Ultrafast charge separation and indirect exciton formation in a MoS₂-MoSe₂ van der Waals heterostructure. *ACS Nano* **2014**, 8 (12), 12717–12724
- (25) Zhu, H.; Wang, J.; Gong, Z.; Kim, Y. D.; Hone, J.; Zhu, X.-Y. Interfacial charge transfer circumventing momentum mismatch at two-dimensional van der Waals heterojunctions. *Nano Lett.* **2017**, *17* (6), 3591–3598.
- (26) Pan, S.; Ceballos, F.; Bellus, M. Z.; Zereshki, P.; Zhao, H. Ultrafast charge transfer between MoTe₂ and MoS₂ monolayers. 2D Mater. **2017**, 4 (1), 015033.
- (27) Ji, Z.; Hong, H.; Zhang, J.; Zhang, Q.; Huang, W.; Cao, T.; Qiao, R.; Liu, C.; Liang, J.; Jin, C. Robust stacking-independent ultrafast charge transfer in MoS₂/WS₂ bilayers. *ACS Nano* **2017**, *11* (12), 12020–12026.
- (28) Zhu, X.; Monahan, N. R.; Gong, Z.; Zhu, H.; Williams, K. W.; Nelson, C. A. Charge transfer excitons at van der Waals interfaces. *J. Am. Chem. Soc.* **2015**, *137* (26), 8313–8320.
- (29) Zheng, Q.; Xie, Y.; Lan, Z.; Prezhdo, O. V.; Saidi, W. A.; Zhao, J. Phonon-coupled ultrafast interlayer charge oscillation at van der Waals heterostructure interfaces. *Phys. Rev. B: Condens. Matter Mater. Phys.* **2018**, *97* (20), 205417.
- (30) Zheng, Q.; Saidi, W. A.; Xie, Y.; Lan, Z.; Prezhdo, O. V.; Petek, H.; Zhao, J. Phonon-assisted ultrafast charge transfer at van der Waals heterostructure interface. *Nano Lett.* **2017**, *17* (10), 6435–6442.
- (31) Li, L.; Long, R.; Prezhdo, O. V. Charge separation and recombination in two-dimensional MoS₂/WS₂: time-domain ab initio modeling. *Chem. Mater.* **2017**, 29 (6), 2466–2473.
- (32) Long, R.; Prezhdo, O. V. Quantum coherence facilitates efficient charge separation at a $MoS_2/MoSe_2$ van der Waals junction. *Nano Lett.* **2016**, *16* (3), 1996–2003.
- (33) Wang, H.; Bang, J.; Sun, Y.; Liang, L.; West, D.; Meunier, V.; Zhang, S. The role of collective motion in the ultrafast charge transfer in van der Waals heterostructures. *Nat. Commun.* **2016**, *7* (1), 1–9.
- (34) Zhang, J.; Hong, H.; Lian, C.; Ma, W.; Xu, X.; Zhou, X.; Fu, H.; Liu, K.; Meng, S. Interlayer-state-coupling dependent ultrafast charge transfer in MoS₂/WS₂ bilayers. *Adv. Sci.* **2017**, *4* (9), 1700086.
- (35) Hedin, L. New method for calculating the one-particle Green's function with application to the electron-gas problem. *Phys. Rev.* **1965**, *139* (3A), A796.
- (36) Hybertsen, M. S.; Louie, S. G. Electron correlation in semiconductors and insulators: Band gaps and quasiparticle energies. *Phys. Rev. B: Condens. Matter Mater. Phys.* **1986**, 34 (8), 5390.
- (37) Rohlfing, M.; Louie, S. G. Electron-hole excitations in semiconductors and insulators. *Phys. Rev. Lett.* **1998**, *81* (11), 2312.
- (38) Gross, E. K. U.; Kohn, W. Local density-functional theory of frequency-dependent linear response. *Phys. Rev. Lett.* **1985**, *55* (26), 2850.
- (39) Marques, M. A.; Maitra, N. T.; Nogueira, F. M.; Gross, E. K.; Rubio, A. Fundamentals of time-dependent density functional theory. Springer Science & Business Media: 2012; Vol. 837.
- (40) Refaely-Abramson, S.; Jain, M.; Sharifzadeh, S.; Neaton, J. B.; Kronik, L. Solid-state optical absorption from optimally tuned time-dependent range-separated hybrid density functional theory. *Phys. Rev. B: Condens. Matter Mater. Phys.* **2015**, 92 (8), No. 081204(R).
- (41) Refaely-Abramson, S.; Sharifzadeh, S.; Jain, M.; Baer, R.; Neaton, J. B.; Kronik, L. Gap renormalization of molecular crystals

- from density-functional theory. Phys. Rev. B: Condens. Matter Mater. Phys. 2013, 88 (8), No. 081204(R).
- (42) Wing, D.; Haber, J. B.; Noff, R.; Barker, B.; Egger, D. A.; Ramasubramaniam, A.; Louie, S. G.; Neaton, J. B.; Kronik, L. Comparing time-dependent density functional theory with manybody perturbation theory for semiconductors: Screened range-separated hybrids and the G W plus Bethe-Salpeter approach. *Phys. Rev. Materials* **2019**, *3* (6), 064603.
- (43) Refaely-Abramson, S.; Sharifzadeh, S.; Govind, N.; Autschbach, J.; Neaton, J. B.; Baer, R.; Kronik, L. Quasiparticle spectra from a nonempirical optimally tuned range-separated hybrid density functional. *Phys. Rev. Lett.* **2012**, *109* (22), 226405.
- (44) Zhang, X.; Li, Z.; Lu, G. A non-self-consistent range-separated time-dependent density functional approach for large-scale simulations. *J. Phys.: Condens. Matter* **2012**, 24 (20), 205801.
- (45) Huang, L.-y.; Zhang, X.; Zhang, M.; Lu, G. Effect of point defects on optical properties of graphene fluoride: a first-principles study. *J. Phys. Chem. C* **2017**, *121* (23), 12855–12862.
- (46) Huang, L.-y.; Zhang, X.; Zhang, M.; Lu, G. Optically inactive defects in monolayer and bilayer phosphorene: A first-principles study. *Phys. Rev. Materials* **2018**, 2 (5), 054003.
- (47) Gao, Y.; Zhang, M.; Zhang, X.; Lu, G. Decreasing exciton binding energy in two-dimensional halide perovskites by lead vacancies. *J. Phys. Chem. Lett.* **2019**, *10* (14), 3820–3827.
- (48) Nan, G.; Zhang, X.; Lu, G. Self-Healing of Photocurrent Degradation in Perovskite Solar Cells: The Role of Defect-Trapped Excitons. *J. Phys. Chem. Lett.* **2019**, *10* (24), 7774–7780.
- (49) Zhang, X.; Li, Z.; Lu, G. First-principles simulations of exciton diffusion in organic semiconductors. *Phys. Rev. B: Condens. Matter Mater. Phys.* **2011**, 84 (23), 235208.
- (50) Casida, M. E., Time-dependent density functional response theory for molecules. In *Recent Advances In Density Functional Methods: (Part I)*; World Scientific: 1995; pp 155–192.
- (51) Tully, J. C. Molecular dynamics with electronic transitions. J. Chem. Phys. 1990, 93 (2), 1061–1071.
- (52) Duncan, W. R.; Craig, C. F.; Prezhdo, O. V. Time-domain ab initio study of charge relaxation and recombination in dye-sensitized TiO2. *J. Am. Chem. Soc.* **2007**, *129* (27), 8528–8543.
- (53) Fischer, S. A.; Habenicht, B. F.; Madrid, A. B.; Duncan, W. R.; Prezhdo, O. V. Regarding the validity of the time-dependent Kohn-Sham approach for electron-nuclear dynamics via trajectory surface hopping. *J. Chem. Phys.* **2011**, *134* (2), 024102.
- (54) Li, Z.; Zhang, X.; Lu, G. Exciton diffusion in disordered small molecules for organic photovoltaics: insights from first-principles simulations. *J. Phys.: Condens. Matter* **2014**, 26 (18), 185006.
- (55) Wu, G.; Li, Z.; Zhang, X.; Lu, G. Charge separation and exciton dynamics at polymer/ZnO interface from first-principles simulations. *J. Phys. Chem. Lett.* **2014**, *5* (15), 2649–2656.
- (56) Kresse, G.; Furthmüller, J. Efficient iterative schemes for ab initio total-energy calculations using a plane-wave basis set. *Phys. Rev. B: Condens. Matter Mater. Phys.* **1996**, *54* (16), 11169.
- (57) Blöchl, P. E. Projector augmented-wave method. Phys. Rev. B: Condens. Matter Mater. Phys. 1994, 50 (24), 17953.
- (58) Perdew, J. P.; Burke, K.; Ernzerhof, M. Generalized gradient approximation made simple. *Phys. Rev. Lett.* **1996**, 77 (18), 3865.
- (59) Grimme, S. Semiempirical GGA-type density functional constructed with a long-range dispersion correction. *J. Comput. Chem.* **2006**, 27 (15), 1787–1799.
- (60) Kośmider, K.; Fernández-Rossier, J. Electronic properties of the MoS₂-WS₂ heterojunction. *Phys. Rev. B: Condens. Matter Mater. Phys.* **2013**, 87 (7), 075451.
- (61) Chen, H.; Wen, X.; Zhang, J.; Wu, T.; Gong, Y.; Zhang, X.; Yuan, J.; Yi, C.; Lou, J.; Ajayan, P. M. Ultrafast formation of interlayer hot excitons in atomically thin MoS₂/WS₂ heterostructures. *Nat. Commun.* **2016**, *7* (1), 1–8.
- (62) Zhang, J.; Hong, H.; Zhang, J.; Fu, H.; You, P.; Lischner, J.; Liu, K.; Kaxiras, E.; Meng, S. New pathway for hot electron relaxation in two-dimensional heterostructures. *Nano Lett.* **2018**, *18* (9), 6057–6063.